PNAS RESEARCH ARTICLE | APPLIED PHYSICAL SCIENCES

Mussel-inspired cross-linking mechanisms enhance gelation and adhesion of multifunctional mucin-derived hydrogels

George D. Degen[a,b,1], Corey A. Stevens[b], Gerardo Cárcamo-Oyarce[b,2], Jake Song[c], Raju Bej[d], Peng Tang[d], Katharina Ribbeck[b], Rainer Haag[d], and Gareth H. McKinley[a]

Affiliations are included on p. 7.

Edited by Matthew Tirrell, The University of Chicago, Chicago, IL; received August 7, 2024; accepted January 8, 2025

Mucus supports human health by hydrating, lubricating, and preventing infection of wet epithelial surfaces. The beneficial material properties and bioactivity of mucus stem from glycoproteins called mucins, motivating the development of mucin-derived hydrogels for wound dressings and antifouling coatings. However, these applications require robust gelation and adhesion to a wide range of substrates. Inspired by the chemical cross-linking and water-tolerant adhesion of marine mussel adhesive structures, we use catechol–thiol bonding to drive gelation of native mucin proteins and synthetic mucin-inspired polymers, forming soft, adhesive hydrogels that can be coated onto diverse surfaces. The gelation dynamics and adhesive properties can be systematically tuned by varying the hydrogel composition, polymer architecture, and thiol availability, with gelation timescales adjustable from seconds to hours, and values of elastic modulus, failure stress, and debonding work spanning orders of magnitude. We demonstrate the functionality of these gels in two applications: as tissue adhesives, using porcine skin as a proxy for human skin, and as bioactive surface coatings to prevent bacterial colonization. The results highlight the potential of catechol–thiol cross-linking as a versatile platform for engineering multifunctional glycoprotein hydrogels with applications in wound repair and antimicrobial surface engineering.

biomaterials | mucus | catechol-thiol bond | tissue adhesive | antifouling

Significance

The layers of mucus coating vulnerable surfaces in the body are composed of lubricious, bioactive proteins called mucins that critically support human health. Many of the beneficial properties of mucins exceed the capabilities of synthetic materials and would be desirable for biomedical applications; however, there remains a need for methods to fabricate mucin-based materials. Here, we present a biologically inspired strategy for achieving adhesive hydrogels from native mucin proteins and synthetic mucin-inspired polymers. By identifying the molecular mechanisms that tune gelation and adhesion, and demonstrating proofs-of-concept for key applications, we provide a general blueprint for engineering soft, multifunctional adhesives for use in the human body.

Wet epithelial surfaces are coated in layers of mucus that hydrate, lubricate, and present a physicochemical barrier protecting the underlying tissue (1). Many of these critical biological functions are attributed to a family of glycosylated proteins called mucins, which assemble into viscoelastic, disulfide-linked networks (2) with bioactive properties (3, 4). The possibility of leveraging the mechanical and biochemical properties of mucins has motivated research on mucin-based biomedical materials (5–7). However, applications such as wound dressings (8), antifouling and lubricious hydrogel coatings (9), and repair of depleted native mucus layers (10) require robust gelation and adhesion to tissue and implant materials in physiological environments, beyond the transient cross-linking (11) and adsorption (12) of native mucins. Enhanced cross-linking of mucin proteins has previously been achieved using disulfide bonding (13) or covalent modification (14, 15), and adhesion of mucin monolayers has been achieved by multistep covalent attachment to surfaces (16, 17), but there remains a need for strategies to simultaneously cross-link and adhere mucin-based hydrogels while preserving mucin bioactivity.

Adhesion in physiological environments, where water undermines adhesive interactions, is a longstanding technological challenge (18). To overcome this challenge, we pursued a biologically inspired strategy for cross-linking and adhesion. Marine mussels adhere to wet surfaces by fabricating a structure called a byssus, a collection of adhesive plaques and energy-dissipating threads composed of proteins rich in 3,4-dihydroxyphenylalanine (Dopa) (19). Dopa and related catechol analogs can participate in a diverse range of intermolecular interactions (20, 21) that contribute to cross-linking and adhesion of the byssus (22, 23), inspiring the design of catechol-based materials including self-healing gels (24), biocompatible coatings (25), and biomedical adhesives (26). Of the interactions formed by catechols, Michael addition of thiols to oxidized catechols occurs rapidly in physiological environments (27) and has previously been shown to enable formation of gels (28–32) and adhesives (33–36). Because cysteine residues account for approximately 5% of the mucin primary structure (37), we hypothesized that catecholic polymers could cross-link mucin proteins by catechol–thiol bonding, while also enabling adhesion to medically relevant surfaces. To test this hypothesis, we investigated a range of thiol-functionalized polymers including 4-arm PEG-thiol (PEG-4SH), a synthetic mucin-inspired polymer (MIP), as well as native mucin proteins (MUC2 and MUC5AC) (Fig. 1*A*), combined with two

Author contributions: G.D.D., C.A.S., G.C.-O., K.R., and G.H.M. designed research; G.D.D. and G.C.-O. performed research; J.S., R.B., and P.T. contributed new reagents; G.D.D. and G.C.-O. analyzed data; and G.D.D., C.A.S., G.C.-O., J.S., R.B., P.T., K.R., R.H., and G.H.M. wrote the paper.

Competing interest statement: G.D.D., C.A.S., K.R., and G.H.M. are inventors on a provisional US patent application (63/639,581) covering a portion of this work.

This article is a PNAS Direct Submission.

Copyright © 2025 the Author(s). Published by PNAS. This article is distributed under Creative Commons Attribution-NonCommercial-NoDerivatives License 4.0 (CC BY-NC-ND).

[1]To whom correspondence may be addressed. Email: gdegen@mit.edu.

[2]Present Address: Área de Biomedicina, Facultad de Ciencias Biológicas, Departamento de Enfermedades Infecciosas del Adulto, Facultad de Medicina, Pontificia Universidad Católica de Chile, Santiago 8320000, Chile.

This article contains supporting information online at https://www.pnas.org/lookup/suppl/doi:10.1073/pnas.2415927122/-/DCSupplemental.

Published February 19, 2025.

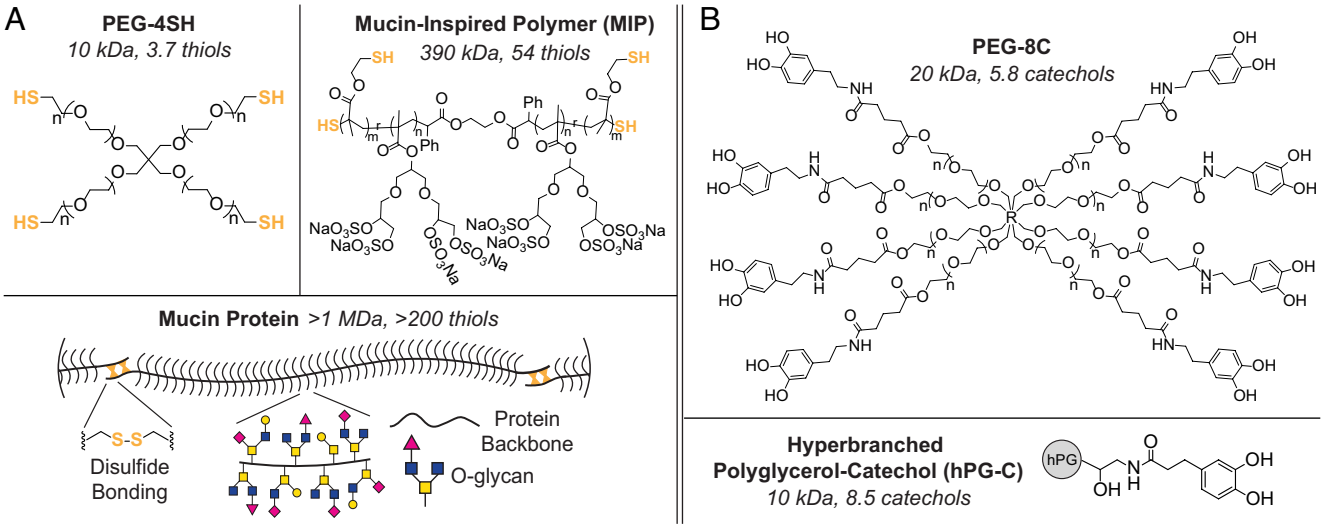

Fig. 1. Schematic overview of the polymers investigated in this work. (*A*) Thiol-functionalized polymers and (*B*) catechol-functionalized cross-linkers. The structures shown are ideal; the average functionalization of thiol or catechol groups per molecule is stated in the image labels.

catechol-functionalized cross-linkers: 8-arm PEG-catechol (PEG-8C) and hyperbranched polyglycerol-catechol (hPG-C) (Fig. 1*B*). We demonstrate that catechol–thiol bonding drives the formation of adhesive hydrogels, with gelation dynamics and adhesive properties tuned by the hydrogel composition, polymer architecture, and availability of thiol functionalities for cross-linking. We further show that our hydrogels adhere to tissue surfaces and discourage bacterial biofilm formation, highlighting the promise of catechol–thiol cross-linking for the design of biomedical materials with applications in wound repair and antimicrobial surface engineering.

Results and Discussion

To investigate the cross-linking of thiolated polymers by catechol–thiol bonding, we first identified reaction conditions enabling gelation of a model thiolated polymer, 4-arm polyethylene glycol-thiol (PEG-4SH), cross-linked by 8-arm PEG-catechol (PEG-8C); see Fig. 1. Catechol–thiol bonding occurs by oxidation of a catechol group to a quinone, followed by Michael addition of a thiol group to the quinone (27). We evaluated three methods of catechol oxidation: enzymatic oxidation by tyrosinase (38), chemical oxidation by periodate (39), and auto-oxidation at pH 9 (28). For each oxidation method, we combined solutions of PEG-4SH and PEG-8C across a range of polymer concentrations and identified the resulting cross-links by gelation experiments, spectroscopy, and mass spectrometry as described in *SI Appendix*, section S6, Table S1, and Figs. S7–S10. We found that specific oxidation of catechols by tyrosinase promoted intermolecular catechol–thiol cross-linking and rapid gelation at low polymer concentrations, whereas nonspecific oxidation by periodate or alkalinity allowed the formation of intramolecular disulfide and dicatechol bonds that slowed or prevented gelation, described in *SI Appendix*, section S7. To demonstrate the generality of our findings, we investigated gelation of a different catechol-functionalized polymer, hPG-C, finding qualitatively similar gelation behavior to PEG-8C upon addition of PEG-4SH (*SI Appendix*, Table S1). Based on these initial results, we selected tyrosinase as the method of catechol oxidation for further gelation studies, using concentrations of PEG-8C (1%) and hPG-C (4%) that were sufficiently dilute to avoid gelation in the absence of PEG-4SH.

To quantitively evaluate gelation by catechol–thiol cross-linking, we combined solutions of PEG-4SH, either PEG-8C or hPG-C, and tyrosinase, and tracked the temporal evolution of the linear viscoelastic storage modulus $G'(\omega, t)$ and loss modulus $G''(\omega, t)$ by small amplitude oscillatory shear rheometry at a fixed frequency ω = 5 rad/s. Fig. 2 *A* and *B* shows the evolution of G' as a function of time t for different concentrations of PEG-4SH cross-linked by (A) PEG-8C and (B) hPG-C. The plots show that G' increases with time as gelation occurs and that the polymer composition influences the gelation rate and stiffness of the resulting gels. The loss modulus G'' remained near the sensitivity limit of the 8 mm diameter rheometer fixture throughout the gelation process ($G'' \leq$ 1 Pa, see *SI Appendix*, Fig. S11) and is omitted for clarity. To characterize the dynamics of the gelation process, we define a characteristic timescale t_{gel} as the time at which G' first exceeds 1 Pa, noting that weak gels may not surpass this threshold and that the low values of G'' preclude the use of other quantitative criteria for identifying gelation (*SI Appendix*, Fig. S11, caption). Following Mours and Winter (40), we quantify the rate of gelation by a mutation timescale $\lambda(t) = \left(\frac{1}{G'}\frac{dG'}{dt}\right)^{-1} = \left(\frac{d\ln G'}{dt}\right)^{-1}$, the inverse of the relative rate of growth of the elastic modulus. The smallest value of mutation timescale, denoted λ^*, therefore identifies the largest relative growth rate of G'. The stiffness of the gels was characterized by the storage modulus $G_{\lambda=3h}$ measured when the rate of gelation had slowed sufficiently for the mutation timescale to exceed 3 h. We report $G_{\lambda=3h}$ rather than the final measured storage modulus G_f to facilitate comparison between experiments in which G' did not reach a final asymptotic value. Fig. 2*C* shows the average values of t_{gel}, λ^*, and $G_{\lambda=3h}$ as functions of the molar ratio of thiols to catechols. The plots are shifted laterally relative to one another due to the higher catechol concentration in 4% hPG-C (34 mM) than in 1% PEG-8C (3 mM), resulting in a lower thiol:catechol ratio for hPG-C at a given concentration of PEG-4SH. For each catecholic cross-linker, the gelation dynamics depended systematically on the composition of the hydrogels. Intermediate thiol:catechol ratios resulted in rapid gelation and minimum values of t_{gel} and λ^*. Higher thiol:catechol ratios slowed gelation, with t_{gel} and λ^* increasing as the thiol:catechol ratio approached 1:1, but ultimately resulted in stiffer gels, with $G_{\lambda=3h}$ increasing by up to four orders of magnitude (0.1 Pa to 1 kPa). Here, the catecholic polymers are sufficiently dilute that no gelation occurs without PEG-4SH. Addition of PEG-4SH at a low thiol:-catechol ratio results in the rapid formation of a sparsely cross-linked polymer network with a short gelation timescale and low modulus. Increasing the concentration of PEG-4SH increases the gelation timescale, likely due to reversible inhibition of the tyrosinase

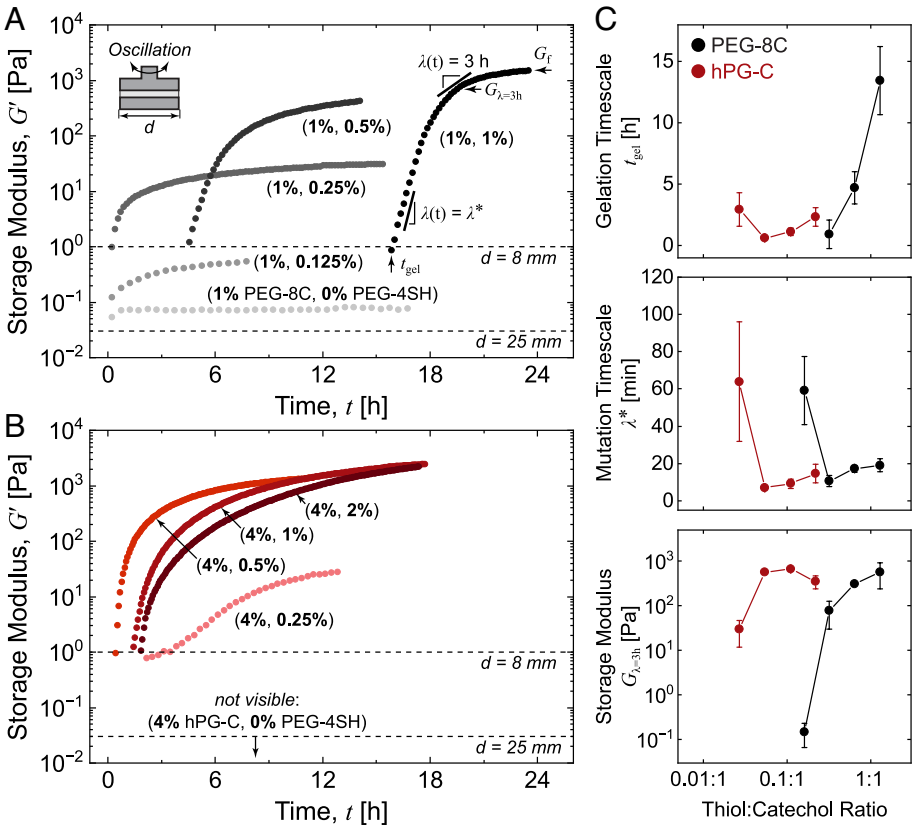

Fig. 2. Gelation dynamics of catechol- and thiol-functionalized polymers. Evolution of the storage modulus G' vs time t at frequency ω = 5 rad/s for (*A*) 1% PEG-8C, 0 to 1% PEG-4SH, 0.16 mg/mL tyrosinase and (*B*) 4% hPG-C, 0 to 2% PEG-4SH, 0.64 mg/mL tyrosinase. The dashed lines show the minimum measurable moduli for different parallel plate test fixtures (diameter d = 8 or 25 mm). The gelation timescale t_{gel}, fastest mutation timescale λ^*, storage modulus $G_{\lambda=3h}$, and final storage modulus G_f are indicated. (*C*) Average values of t_{gel}, λ^*, and $G_{\lambda=3h}$ as a function of the thiol:catechol ratio ($N \geq 3$); error bars show the SD.

enzyme by PEG-4SH (41), but ultimately leads to gels with a larger final modulus as the catechols oxidize and cross-link with thiols. With a mechanistic understanding of gelation in hand, we next investigated the adhesive properties of the hydrogels.

Adhesion of hydrogels to surfaces is important for biomedical applications such as surgical adhesives (42) and coatings for catheters and stents (16). The stainless-steel test fixtures of the rheometer possess a metal oxide passivating layer similar to implant materials, making them useful model surfaces for adhesion studies. To quantitatively assess the adhesive properties of the hydrogels, we measured the normal force $F(t)$ and the separation distance $h(t)$ between the rheometer plates while separating the plates at a constant velocity ($dh/dt = 100\ \mu m/s$). Fig. 3 *A* and *B* shows the tensile engineering stress $\sigma = 4F/\pi d^2$ as a function of the engineering strain $\varepsilon = (h - h_0)/h_0$, measured immediately after gelation. We characterize the stress–strain curves by the failure stress σ_f, equal to the largest tensile engineering stress measured during separation, and the debonding work W_d, calculated as the integrated area under the stress–strain curve, with dimensions of energy per volume. Like the gelation dynamics, the adhesive properties of the hydrogels depended systematically on the gel composition. As shown in Fig. 3*C*, the average values of failure stress and debonding work were positively correlated with the thiol:catechol ratio, as well as with the final modulus G_f of the gels (*SI Appendix*, Fig. S12). We note that the failure stress greatly exceeded G_f due to the highly confined geometry, characterized by the ratio of the rheometer plate diameter to the initial hydrogel thickness (d/h_0 = 40), discussed in *SI Appendix*, section S8.

To interpret the relationships between hydrogel composition, modulus, and adhesion, we considered possible failure modes of the hydrogels during separation of the surfaces. Failure can occur within the bulk of the gel (cohesive failure) or at the gel–substrate interface (adhesive failure) (43). As discussed in *SI Appendix*, section S8 and Figs. S12 and S13, catechol–thiol bonds strengthen cohesion by increasing the gel modulus. Moreover, we find that catechols enhance the hydrogel failure stress by up to 50% relative to control gels of the same modulus, suggesting that catechols also strengthen the adhesive interface. Catechols may form bidentate hydrogen bonds or coordination bonds (21) at the gel–steel interface, noting that hydrogen bonding and metal coordination can delay the catechol oxidation (44, 45) that reduces interfacial adhesion (46). Catechol–thiol adducts may also contribute to adhesion, although the molecular mechanisms of adduct surface binding have not been explored. Regardless of the specific mechanism, our results demonstrate that catechols enhance adhesive performance by contributing to both adhesion and cohesion of the hydrogels.

Having demonstrated catechol-based cross-linking and adhesion of model thiolated polymers, we tested our cross-linking approach using polymers of molecular weight and thiol content more similar to native mucin proteins. We synthesized a mucin-inspired polymer (MIP) of high molecular weight (390 kDa), functionalized with thiol groups and dendronized, sulfated polyglycerol. Fig. 4 *A* and *B* shows that combining the MIP with 1% PEG-8C and tyrosinase (MIP, blue) resulted in rapid gelation (t_{gel} < 1 min) and substantial adhesion. Unlike the hydrogels composed of PEG-4SH, the storage modulus of the MIP-based gels reached a plateau during our experiments; we therefore report the average values of the final modulus G_f, as well as the failure stress σ_f and debonding work W_d, in Fig. 4*C*. Doubling the concentration of MIP (2x MIP, dark blue), corresponding to an increase in thiol:catechol ratio from 0.7:1 to 1.4:1, doubled the value of G_f and increased σ_f by 50%, without measurably

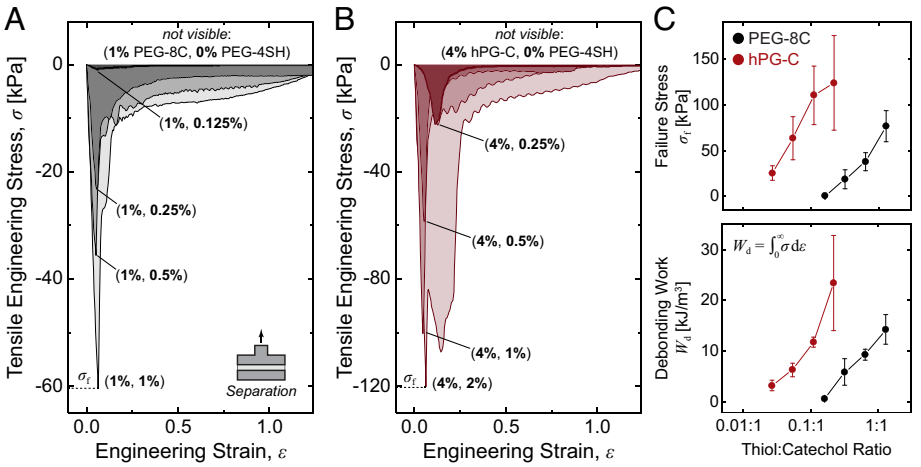

Fig. 3. Adhesion of hydrogels composed of catechol- and thiol-functionalized polymers measured after the gelation shown in Fig. 2. (*A*) Evolution of the tensile engineering stress σ vs engineering strain ε for hydrogels composed of PEG-4SH cross-linked by (*A*) PEG-8C and (*B*) hPG-C, where negative stresses correspond to tension. The largest tensile engineering stress is denoted the failure stress σ_f, and the integrated area under the stress–strain curve gives the debonding work W_d. (*C*) Average values of σ_f and W_d as a function of the catechol:thiol ratio ($N \geq 3$); error bars show the SD.

affecting the gelation timescale. Compared with the hours-long gelation timescale of PEG-4SH hydrogels at thiol:catechol ratios approaching 1:1, the gelation of MIP in seconds indicates that the larger molecular weight and greater thiol functionalization of the MIP relative to PEG-4SH promotes the formation of a sample-spanning network, thereby demonstrating that the gelation dynamics of catechol–thiol hydrogels can be tuned from seconds to hours by the molecular architecture of the constituent polymers.

Based on the similar molecular weight and thiol content of mucin proteins to the MIP, we anticipated that catecholic cross-linkers could drive mucin gelation and adhesion. However, because native mucins polymerize by disulfide bonding (2), we hypothesized that reduction of mucin disulfide bonds would be necessary to enable catechol–thiol cross-linking. To test this hypothesis, we purified mucins from porcine intestines (mainly MUC2) and chemically reduced the disulfide bonds for comparison with as-purified mucin. Fig. 4 *A*–*C* shows that combining as-purified or reduced mucin with 1% PEG-8C and tyrosinase resulted in the formation of hydrogels with different properties. Relative to gels composed of as-purified mucin (MUC2, light orange), gels composed of reduced mucin ($MUC2_r$, orange) formed more quickly (ten-fold lower values of t_{gel}) and showed five-fold increases in final modulus and failure stress, as well as a slightly higher value of debonding work. The modulus and adhesive properties were further increased by doubling the concentration of reduced mucin (2x

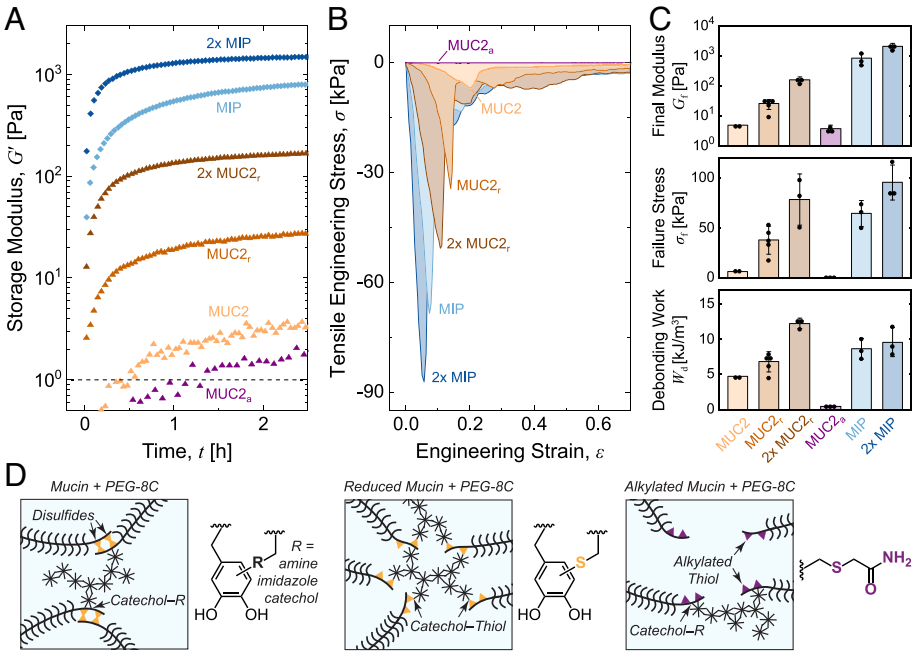

Fig. 4. Gelation and adhesion of 1.4% or 2.8% (2x) MIP or mucin protein (MUC2) cross-linked by 1% PEG-8C and 0.16 mg/mL tyrosinase. Subscripts indicate reduction "r" or alkylation "a" of mucin. (*A*) Evolution of the storage modulus G' vs time t at frequency $\omega = 5$ rad/s. Dashed line shows the minimum measurable modulus for the parallel plate test fixture ($d = 8$ mm). (*B*) Evolution of the tensile engineering stress σ vs engineering strain ε measured after gelation. (*C*) Average values of the final modulus G_f, failure stress σ_f, and debonding work W_d ($N \geq 2$); error bars show the SD for $N \geq 3$. (*D*) Sketches of the proposed cross-linking of different preparations of mucin proteins by PEG-8C in the presence of tyrosinase. 8-spoked asterisks represent PEG-8C. Yellow triangles represent thiol groups, merged yellow triangles represent disulfide bonds, and purple triangles represent alkylated thiol groups. Cross-linking between catechol groups and either amine, imidazole, or other catechol groups is proposed to contribute to gelation regardless of mucin preparation, whereas catechol–thiol cross-linking requires reduced thiol groups, and is prevented by disulfide bonding or thiol alkylation.

$MUC2_r$, dark orange). To confirm the involvement of thiols in cross-linking, we showed that alkylation of mucin thiols weakened gelation ($MUC2_a$, purple triangles), presumably by preventing catechol–thiol bonding. Finally, control measurements of as-purified or reduced mucin with tyrosinase but without PEG-8C showed only weak gelation and adhesion (*SI Appendix*, Fig. S14), consistent with the role of catechols in cross-linking.

Although the gelation results indicate that reduced mucin proteins can be cross-linked by catechol–thiol bonds, the gelation of as-purified and alkylated mucin suggests that PEG-8C can form additional cross-links with mucin. Catechol–amine, catechol–imidazole, or dicatechol cross-links likely contribute to gelation, given that lysine, histidine, and tyrosine each constitute ~2% of the mucin primary structure (37) and that tyrosine can be oxidized to Dopa by tyrosinase (20). Based on the hydrogel moduli shown in *SI Appendix*, Table S2, and the proportionality between modulus and cross-linking density predicted by the affine network model of polymer gelation (47), we estimate that catechol–thiol bonds account for approximately 80% of the cross-links in gels composed of 1.4% reduced MUC2 and 1% PEG-8C, with other types of bonds accounting for the remainder of the cross-links. Sketches of the proposed cross-linking mechanisms for different preparations of mucin are shown in Fig. 4*D*, emphasizing the dependence of gelation on the availability of mucin thiols for cross-linking.

We next tested the generality of our cross-linking approach using mucin purified from porcine stomachs (mainly MUC5AC, also a major component of pulmonary mucus), noting that mucins from different biological niches can exhibit different physical and biochemical properties (1). Combining reduced MUC5AC with PEG-8C and tyrosinase resulted in gelation in minutes, albeit to a lower final modulus than the values measured for MUC2 (*SI Appendix*, Fig. S14). By contrast, commercial bovine submaxillary mucin (BSM) was not observed to form gels under the same cross-linking conditions (*SI Appendix*, Fig. S14), highlighting the importance of in-lab mucin purification to avoid the harsh processing conditions that degrade commercial mucin (48). To further demonstrate generality, we showed that hyperbranched polyglycerol-catechol (hPG-C) cross-linked and adhered MIPs and native mucin proteins (*SI Appendix*, Fig. S15), finding slower gelation timescales than the same polymers cross-linked by PEG-8C, but similar values of storage modulus and adhesive properties.

A key advantage of our materials design strategy is the potential to develop multifunctional hydrogels that combine the adhesive properties of catechols (26) with the tunable properties of MIPs (49) or the bioactivity of mucins (3, 4) for applications such as surgical adhesives and antifouling coatings. To assess the capacity of our materials to bind to tissue, we deposited hydrogel precursor solutions composed of MIP, PEG-8C, and tyrosinase between moistened pigskin disks glued to the plates of the rheometer test fixture. To partially mitigate variations in thickness across the gel, a gap of $h_0 \approx 1$ mm between the skin surfaces was used, larger than the gap used for the smooth machined steel surfaces. After curing the gels for 1 h (Fig. 5*A*, *Upper Inset*), the surfaces were separated axially to measure the adhesion. Fig. 5*A* shows the tensile engineering stress σ vs engineering strain ε for the MIP-based hydrogels (blue). The adhesion measurements show an average failure stress of $\sigma_f = 10 \pm 4$ kPa ($N = 3$), with a positive correlation between the final modulus and the failure stress of each replicate (Fig. 5*A*, *Lower Inset*). The average failure stress is within the range of values reported for other catechol-functionalized tissue adhesives (1 to 200 kPa) (50) and commercial tissue adhesives (10 to 40 kPa) (51), while somewhat less than state-of-the-art biomedical adhesives (20 to 120 kPa) (51), although we note that the reported values of the failure stress depend on the specific method of adhesion testing (e.g., lap shear, tensile testing) (52). Control measurements of PEG-4SH gels of a similar modulus to the MIP-based gels, but cross-linked by disulfide bonding, showed a lower average failure stress of $\sigma_f = 3 \pm 1$ kPa ($N = 3$) (Fig. 5*A*, gray/black) and a different apparent failure mode. The MIP-based gels failed cohesively in the bulk of the gel, whereas the PEG-4SH gels failed adhesively at the gel–tissue interface (*SI Appendix*, Fig. S16), indicating that the catechol groups in the MIP-based gels bind to the skin surface and discourage adhesive failure. Nevertheless, the MIP-based gels showed weaker adhesion to pigskin than to steel (Fig. 4), likely due to the larger initial gap between the tissue surfaces and lower degree of confinement ($d/h_0 \approx 8$); the influence

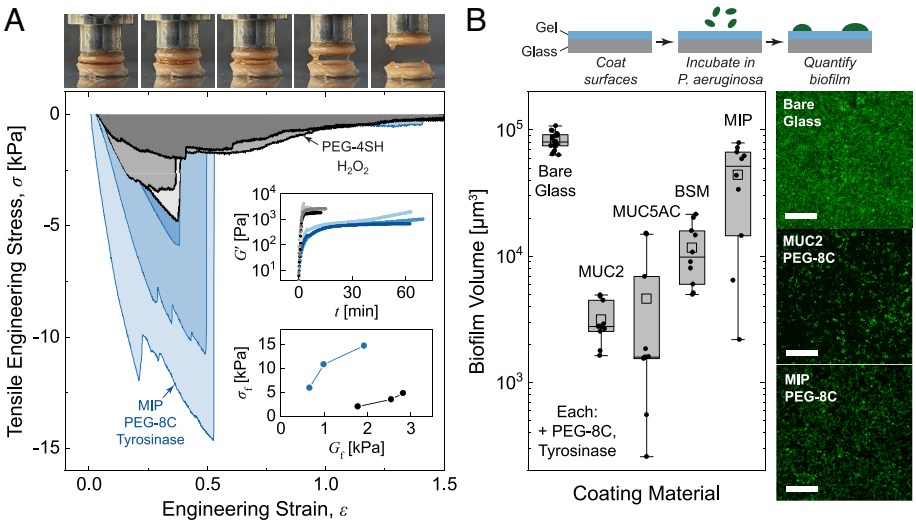

Fig. 5. Applications of mucin-inspired and mucin-derived hydrogels as tissue adhesives and antifouling coatings. (*A*) Adhesion measurements of hydrogels composed of MIP, PEG-8C, and tyrosinase (blue) after gelation between moistened pigskin surfaces. Control measurements of PEG-4SH gels (gray/black) cross-linked by disulfide bonds are shown for comparison. Three replicates for each gel are shown, indicated by different shadings. The *Upper Inset* shows the evolution of the storage modulus G' vs time t at frequency $\omega = 5$ rad/s during gelation of each replicate; the lower inset shows the correlation between the failure stress σ_f and the final storage modulus G_f of the replicates. (*B*) Box plot representation of biofilm volume on bare or coated glass surfaces after incubation in *Pseudomonas aeruginosa*, for coatings composed of in-lab purified mucin (MUC2, MUC5AC), commercial BSM, and MIP, each cross-linked by PEG-8C and tyrosinase. Open squares show the mean of each dataset. Representative fluorescence images are shown on *Right*. (Scale bars, 50 μm.)

of confinement on adhesion is discussed in *SI Appendix*, section S8. We also tested the tissue adhesion of mucin-based hydrogels cross-linked by PEG-8C (*SI Appendix*, Fig. S17), finding lower values of failure stress than the MIP-based or PEG-4SH gels, likely because the lower modulus of the mucin-based gels enables cohesive failure. Collectively, our results indicate that the adhesive performance of both the MIP- and mucin-based gels could be improved by toughening the gels, for example, by incorporating energy dissipating cross-links or hierarchical structures (53), as has been achieved for other protein-based hydrogels (54).

In addition to tissue adhesion, our materials design strategy offers the possibility of reproducing the bioactive properties of mucus such as the ability to discourage biofouling by altering microbial gene expression to prevent attachment to surfaces and disperse existing biofilms (3, 4). To evaluate the antifouling properties of our materials, we coated glass surfaces with mucin-based hydrogels composed of either MUC2 or MUC5AC, each cross-linked by PEG-8C and tyrosinase. We also tested coatings composed of commercial BSM and MIP under the same cross-linking conditions, noting that BSM was not observed to form gels under these conditions (*SI Appendix*, Fig. S14). We incubated the coated surfaces overnight in *P. aeruginosa*, a biofilm-forming pathogen associated with medical device infections (55), and then measured the volume of biofilm on the surfaces by confocal microscopy. Fig. 5*B* shows that the gel coatings composed of native MUC2 and MUC5AC reduced the median biofilm volume by 97 and 98%, respectively, relative to the biofilm volume measured on bare glass. Lesser reductions in biofilm volume were observed for coatings composed of BSM (88%) and MIP (36%). The decreases in biofilm volume cannot be attributed to coating toxicity because the coatings do not alter *P. aeruginosa* viability relative to medium alone (*SI Appendix*, Fig. S18*A*). No reduction in biofilm volume was observed after incubating the surfaces in solutions of native mucin without PEG-8C (*SI Appendix*, Fig. S18*B*), indicating that the PEG-8C enables retention of the mucin on the glass surface. Moreover, the results for BSM indicate that PEG-8C can retain mucin on glass even in the absence of gelation. Nevertheless, the gel coatings composed of native MUC2 and MUC5AC showed superior antifouling performance to the coatings composed of commercial BSM or synthetic MIP, consistent with the ability of mucins to downregulate genes associated with biofilm formation in *P. aeruginosa* (3). The results are particularly promising, given that previous mucin-based coatings that repel other bacteria have failed to reduce biofilm formation of *P. aeruginosa* (17, 56). Moreover, existing methods for depositing mucin-based coatings involve multiple steps (16) or are limited to hydrophobic substrates (5), whereas our gel coatings can be applied in a single step, and are expected to be compatible with both hydrophobic and hydrophilic substrates based on the broad adhesive properties of catechols (21).

Conclusions

We have demonstrated that catechol-functionalized cross-linkers enable gelation and adhesion of thiolated polymers including multiarm PEG-thiol, a synthetic MIP, and purified mucin proteins, with gelation driven by covalent catechol–thiol cross-linking. The hydrogel composition, polymer architecture, and thiol availability were shown to systematically tune the gelation dynamics and adhesive properties, including gelation and mutation timescales, elastic modulus, and failure stress and debonding work. The hydrogels adhere to tissue surfaces and discourage bacterial biofilm formation, raising the possibility of developing biocompatible surgical adhesives and antifouling gel coatings. Future work will seek to leverage additional physico-chemical properties of mucin proteins including lubricity and immune modulation (5). We will also target other thiol-rich biopolymers such as keratin and pursue strategies for targeted underwater adhesive deposition such as coacervation of the adhesive polymers (57), with a goal of developing a family of sustainable, biologically derived, multifunctional materials.

Materials and Methods

Synthesis of 4-arm PEG-thiol (PEG-4SH, 10 kDa, 3.7 thiols/molecule), mucin-inspired polymer (MIP, 390 kDa, 54 thiols/molecule), 8-arm PEG-catechol (PEG-8C, 20 kDa, 5.8 catechols/molecule), and hyperbranched polyglycerol-catechol (hPG-C, 10 kDa, 8.5 catechols/molecule) is described in *SI Appendix*, sections S1–S4 and Figs. S1–S6. Mucin proteins were purified from porcine intestines and stomachs (largely MUC2 and MUC5AC, respectively) following established protocols (58), lyophilized, and stored at −20 °C before use. Lyophilized mucin was solubilized in ultrapure water, shaking at 4 °C overnight. Commercial bovine submaxillary mucin (BSM, Sigma-Aldrich) was solubilized and used without further purification. Mucins and MIPs were reduced or alkylated, flash-frozen, and stored at −80 °C as described in *SI Appendix*, section S5. Tyrosinase (6,540 units/mg, Sigma Aldrich) was prepared at 1.6 mg/mL in 40 mM phosphate buffer, pH 7, 20% glycerol, and stored in flash-frozen aliquots at −80 °C. Hydrogel precursor solutions were prepared from stock solutions of polymers (final concentrations reported as % w/v) and buffer (final buffer conditions 50 mM phosphate, pH 7). Catechols were oxidized by tyrosinase (0.16 to 0.64 mg/mL), periodate (1:1 catechol: periodate), or auto-oxidation (pH 9, 50 mM carbonate buffer). For enzymatic oxidation or auto-oxidation, the polymer solution was briefly bubbled with oxygen gas produced by catalase-induced decomposition of hydrogen peroxide. For control measurements of PEG-4SH gels, thiols were oxidized to disulfide bonds by hydrogen peroxide (0.4−4:1 H_2O_2:thiol).

Gelation was measured with a strain-controlled rheometer (ARES-G2, TA Instruments, New Castle, DE) using parallel plate test fixtures (diameter d = 8 mm, separation distance h_0 = 200 μm, or d = 25 mm, h_0 = 250 μm). Gel precursor solution was injected between the plates, excess solution was trimmed, and mineral oil was placed around the outer rim of the plates to prevent evaporation of the sample. The storage and loss moduli $G'(\omega, t)$ and $G''(\omega, t)$ were measured as functions of time t by small-amplitude oscillatory shear at a fixed frequency (ω = 5 rad/s) and strain amplitude (γ_0 = 0.1), with minimum measurable moduli of 1 Pa (d = 8 mm) and 0.03 Pa (d = 25 mm). To measure adhesion of the gels to tissue, circular sections of pig skin (8 mm diameter) were attached to the rheometer plates with cyanoacrylate glue (Krazy Glue). Skin surfaces were soaked in water for at least 5 min and then blotted with a paper towel, at which point hydrogel precursor solution (1.4% MIP, 1% PEG-8C, 0.16 mg/mL tyrosinase) was injected into the gap between the pigskin surfaces (h_0 = 1 mm). 5 min after injection, the sample area was flooded with water. Hydrogels were cured between the surfaces for 1 h before measuring adhesion. Control gels (4% PEG-4SH, 4:1 H_2O_2:thiol) were cured for at least 5 min before measuring adhesion.

To assess antibiofouling properties of the hydrogels, an overnight culture of *P. aeruginosa* WT strain PAO1, carrying pBBR1(MCS5)-pLac-GFP for constitutive green fluorescent protein (GFP) expression (59), was prepared in Luria Broth (LB, Difco) supplemented with 30 μg/mL gentamicin to maintain the plasmid, with shaking at 37 °C. Wells of a glass-bottom 96-well plate (Celvis) were coated with 20 μL of 1% PEG-8C, 0.16 mg/mL tyrosinase, and a reduced polymer, either MUC2 (0.7%) or MUC5AC, BSM, or MIP (each at 1.4%). Plates were centrifuged at 100×g for 5 min immediately after the addition of the hydrogel precursor solution to obtain a uniform coating. The plate was soaked in water for 20 min, followed by removal of the water and sterilization by ultraviolet light radiation for 1 h. Overnight cultures were diluted in fresh LB medium to an initial OD600 of 0.01, added to the plate, and incubated for 24 h at 37 °C. Viable dispersed cells were quantified via counts of the colony-forming units on LB agar plates. The supernatant containing nonadherent cells was removed from the plate, and the biofilm remaining in each well was washed at least three times with fresh LB. Adhered cells were imaged by confocal microscopy. Image acquisition was performed using a confocal laser scanning microscope (LSM 800; Zeiss) equipped with a 20×/0.5 NA dry objective with 2x digital zoom at an excitation wavelength of 488 nm.

Images were analyzed with the Zeiss ZEN 2.1 imaging software (Thornwoods, NY). Biofilm quantification was performed using BiofilmQ (60).

Data, Materials, and Software Availability. All study data are included in the article and/or *SI Appendix*.

ACKNOWLEDGMENTS. This work was supported by NIH through the MIT Center for Environmental Health Sciences (NIH Training Grant T32–ES007020 and NIH P30–ES002109), the NSF grant no. EF2125118, the Army Research Office through the Institute for Collaborative Biotechnologies ICB–2024–BEM–10 under award W911NF1920026, and the Army Research Office MURI award W911NF2210185. The views and conclusions contained in this document are those of the authors and should not be interpreted as representing the official policies, either expressed or implied, of the Army Research Office or the U.S. Government. The U.S. Government is authorized to reproduce and distribute reprints for Government purposes notwithstanding any copyright notation herein. R.B. and R.H. were funded by the Deutsche Forschungsgemeinschaft (DFG, German Research Foundation) – Project ID 431232613 – SFB 1449. C.A.S. was supported by the Canadian Institutes of Health Research postdoctoral fellowship (MFE–187894). The work was performed in part in the MIT.nano Characterization Facilities. We thank the Biopolymers and Proteomics Core Facility within the Koch Institute's Robert A. Swanson (1969) Biotechnology Center for technical support.

Author affiliations: [a]Department of Mechanical Engineering, Massachusetts Institute of Technology, Cambridge, MA 02139; [b]Department of Biological Engineering, Massachusetts Institute of Technology, Cambridge, MA 02139; [c]Department of Materials Science and Engineering, Massachusetts Institute of Technology, Cambridge, MA 02139; and [d]Institut für Chemie und Biochemie, Freie Universität Berlin, Berlin 14195, Germany

1. C. E. Wagner, K. M. Wheeler, K. Ribbeck, Mucins and their role in shaping the functions of mucus barriers. *Annu. Rev. Cell Dev. Biol.* **34**, 189–215 (2018).
2. J. Carpenter *et al.*, Assembly and organization of the N-terminal region of mucin MUC5AC: Indications for structural and functional distinction from MUC5B. *Proc. Natl. Acad. Sci. U.S.A.* **118**, e2104490118 (2021).
3. K. M. Wheeler *et al.*, Mucin glycans attenuate the virulence of Pseudomonas aeruginosa in infection. *Nat. Microbiol.* **4**, 2146–2154 (2019).
4. J. Takagi *et al.*, Mucin O-glycans are natural inhibitors of Candida albicans pathogenicity. *Nat. Chem. Biol.* **18**, 762–773 (2022).
5. G. Petrou, T. Crouzier, Mucins as multifunctional building blocks of biomaterials. *Biomater. Sci.* **6**, 2282–2297 (2018).
6. M. Marczynski, C. Kimna, O. Lieleg, Purified mucins in drug delivery research. *Adv. Drug Deliv. Rev.* **178**, 113845 (2021).
7. R. Bej, R. Haag, Mucus-inspired dynamic hydrogels: Synthesis and future perspectives. *J. Am. Chem. Soc.* **144**, 20137–20152 (2022).
8. L. Zhang, M. Liu, Y. Zhang, R. Pei, Recent progress of highly adhesive hydrogels as wound dressings. *Biomacromolecules* **21**, 3966–3983 (2020).
9. J. Liu, S. Qu, Z. Suo, W. Yang, Functional hydrogel coatings. *Natl. Sci. Rev.* **8**, nwaa254 (2021).
10. D. Li *et al.*, Growth factors-loaded temperature-sensitive hydrogel as biomimetic mucus attenuated murine Ulcerative colitis via repairing the mucosal barriers. *ACS Appl. Mater. Interfaces* **16**, 7686–7699 (2024).
11. O. W. Meldrum *et al.*, Mucin gel assembly is controlled by a collective action of non-mucin proteins, disulfide bridges, Ca2+ -mediated links, and hydrogen bonding. *Sci. Rep.* **8**, 1–16 (2018).
12. L. Shi, K. D. Caldwell, Mucin adsorption to hydrophobic surfaces. *J. Colloid Interface Sci.* **224**, 372–381 (2000).
13. K. Joyner, D. Song, R. F. Hawkins, R. D. Silcott, G. A. Duncan, A rational approach to form disulfide linked mucin hydrogels. *Soft Mater.* **15**, 9632–9639 (2019).
14. C. V. Duffy, L. David, T. Crouzier, Covalently-crosslinked mucin biopolymer hydrogels for sustained drug delivery. *Acta Biomater.* **20**, 51–59 (2015).
15. K. Jiang *et al.*, Modulating the bioactivity of mucin hydrogels with crosslinking architecture. *Adv. Funct. Mater.* **31**, 2008428 (2021).
16. J. Song, T. M. Lutz, N. Lang, O. Lieleg, Bioinspired dopamine/mucin coatings provide lubricity, wear protection, and cell-repellent properties for medical applications. *Adv. Healthc. Mater.* **10**, 2000831 (2021).
17. B. Winkeljann *et al.*, Covalent mucin coatings form stable anti-biofouling layers on a broad range of medical polymer materials. *Adv. Mater. Interfaces* **7**, 1902069 (2020).
18. B. P. Lee, P. B. Messersmith, J. N. Israelachvili, J. H. Waite, Mussel-inspired adhesives and coatings. *Annu. Rev. Mater. Res.* **41**, 99–132 (2011).
19. J. H. Waite, Mussel adhesion – essential footwork. *J. Exp. Biol.* **220**, 517–530 (2017).
20. J. Yang,M. A. Cohen Stuart, M. Kamperman, Jack of all trades: Versatile catechol crosslinking mechanisms. *Chem. Soc. Rev.* **43**, 8271–8298 (2014).
21. J. Saiz-Poseu, J. Mancebo-Aracil, F. Nador, F. Busqué, D. Ruiz-Molina, The chemistry behind catechol-based adhesion. *Angew. Chemie - Int. Ed.* **58**, 696–714 (2019).
22. Q. Lin *et al.*, Adhesion mechanisms of the mussel foot proteins mfp-1 and mfp-3. *Proc. Natl. Acad. Sci. U.S.A.* **104**, 3782–6 (2007).
23. T. Priemel *et al.*, Compartmentalized processing of catechols during mussel byssus fabrication determines the destiny of DOPA. *Proc. Natl. Acad. Sci. U.S.A.* **117**, 7613–7621 (2020).
24. N. Holten-Andersen *et al.*, pH-induced metal-ligand cross-links inspired by mussel yield self-healing polymer networks with near-covalent elastic moduli. *Proc. Natl. Acad. Sci. U.S.A.* **108**, 2651–2655 (2011).
25. Z. Yang *et al.*, Bioclickable and mussel adhesive peptide mimics for engineering vascular stent surfaces. *Proc. Natl. Acad. Sci. U.S.A.* **117**, 16127–16137 (2020).
26. W. Zhang *et al.*, Catechol-functionalized hydrogels: Biomimetic design, adhesion mechanism, and biomedical applications. *Chem. Soc. Rev.* **49**, 433–464 (2020).
27. Y. Li, S. Jongberg, M. L. Andersen, M. J. Davies, M. N. Lund, Quinone-induced protein modifications: Kinetic preference for reaction of 1,2-benzoquinones with thiol groups in proteins. *Free Radic. Biol. Med.* **97**, 148–157 (2016).
28. Z. Guo, S. Mi, W. Sun, The multifaceted nature of catechol chemistry: Bioinspired pH-initiated hyaluronic acid hydrogels with tunable cohesive and adhesive properties. *J. Mater. Chem. B* **6**, 6234–6244 (2018).
29. C. Y. Lin, J. C. Liu, J. C. Liu, Comparison between catechol- and thiol-based adhesion using elastin-like polypeptides. *ACS Appl. Bio Mater.* **3**, 3894–3905 (2020).
30. Y. Lee *et al.*, Thermo-sensitive, injectable, and tissue adhesive sol-gel transition hyaluronic acid/pluronic composite hydrogels prepared from bio-inspired catechol-thiol reaction. *Soft Matter* **6**, 977–983 (2010).
31. J. H. Ryu *et al.*, Catechol-functionalized chitosan/pluronic hydrogels for tissue adhesives and hemostatic materials. *Biomacromolecules* **12**, 2653–2659 (2011).
32. H. S. Kim, H. O. Ham, Y. J. Son, P. B. Messersmith, H. S. Yoo, Electrospun catechol-modified poly(ethyleneglycol) nanofibrous mesh for anti-fouling properties. *J. Mater. Chem. B* **1**, 3940–3949 (2013).
33. C. Y. Choi *et al.*, Organic transformation of lignin into mussel-inspired glues: Next-generation 2K adhesive for setting corals under saltwater. *Green Chem.* **26**, 2044–2058 (2023).
34. C. M. Schröter, L. D. Bangert, H. G. Börner, Enhancing adhesion properties of commodity polymers through thiol-catechol connectivities: A case study on polymerizing polystyrene-telechelics via thiol-quinone michael-polyaddition. *ACS Macro Lett.* **13**, 440–445 (2024).
35. T. J. Neubert *et al.*, Redox-triggered debonding of mussel-inspired pressure sensitive adhesives: Improving efficiency through functional design. *Angew. Chemie - Int. Ed.* **63**, e202408441 (2024).
36. Y. Xie *et al.*, Injectable self-healing alginate/PEG hydrogels cross-linked via thiol-Michael addition bonds for hemostasis and wound healing. *Carbohydr. Polym.* **348**, 122864 (2025).
37. A. Bateman *et al.*, UniProt: The universal protein knowledgebase in 2023. *Nucleic Acids Res.* **51**, D523–D531 (2023).
38. S. Ito, G. Prota, A facile one-step synthesis of cysteinyldopas using mushroom tyrosinase. *Experientia* **33**, 1118–1119 (1977).
39. J. M. Kohn, J. Riedel, J. Horsch, H. Stephanowitz, H. G. Börner, Mussel-inspired polymerization of peptides: The chemical activation route as key to broaden the sequential space of artificial mussel-glue proteins. *Macromol. Rapid Commun.* **41**, 1900431 (2020).
40. M. Mours, H. H. Winter, Time-resolved rheometry. *Acta Rheol Acta* **33**, 385–397 (1994).
41. S. Naish-Byfield, C. J. Cooksey, P. A. Riley, Oxidation of monohydric phenol substrates by tyrosinase: Effect of dithiothreitol on kinetics. *Biochem. J.* **304**, 155–162 (1994).
42. R. Pinnaratip, M. S. A. Bhuiyan, K. Meyers, R. M. Rajachar, B. P. Lee, Multifunctional biomedical adhesives. *Adv. Healthc. Mater.* **8**, 1–17 (2019).
43. A. J. Crosby, K. R. Shull, H. Lakrout, C. Creton, Deformation and failure modes of adhesively bonded elastic layers. *J. Appl. Phys.* **88**, 2956–2966 (2000).
44. T. H. Anderson *et al.*, The contribution of DOPA to substrate-peptide adhesion and internal cohesion of mussel-inspired synthetic peptide films. *Adv. Funct. Mater.* **8**, 4196–4205 (2010).
45. D. E. Fullenkamp, D. G. Barrett, D. R. Miller, J. W. Kurutz, P. B. Messersmith, pH-dependent cross-linking of catechols through oxidation via Fe 3+ and potential implications for mussel adhesion *RSC Adv.* **4**, 25127–25134 (2014).
46. J. Yu *et al.*, Effects of interfacial redox in mussel adhesive protein films on mica. *Adv. Mater.* **23**, 2362–2366 (2011).
47. L. R. G. Treloar, *The Physics of Rubber Elasticity* (Oxford University Press, 1975).
48. C. E. Wagner *et al.*, Comparison of physicochemical properties of native mucus and reconstituted mucin gels. *Biomacromolecules* **24**, 628–639 (2023).
49. R. E. Detwiler, J. R. Kramer, Preparation and applications of artificial mucins in biomedicine. *Curr. Opin. Solid State Mater. Sci.* **26**, 1–33 (2022).
50. W. Y. Quan *et al.*, Mussel-inspired catechol-functionalized hydrogels and their medical applications. *Molecules* **24**, 2586 (2019).
51. H. Yuk *et al.*, Dry double-sided tape for adhesion of wet tissues and devices. *Nature* **575**, 169–174 (2019).
52. S. S. Scherrer, P. F. Cesar, M. V. Swain, Direct comparison of the bond strength results of the different test methods: A critical literature review. *Dent. Mater.* **26**, e78 (2010).
53. X. Li, J. P. Gong, Design principles for strong and tough hydrogels. *Nat. Rev. Mater.* **9**, 380–398 (2024).
54. M. Wang, S. Sun, G. Dong, F. Long, J. T. Butcher, Soft, strong, tough, and durable protein-based fiber hydrogels. *Proc. Natl. Acad. Sci. U.S.A.* **120**, e2213030120 (2023).
55. J. Yadav, R. M. Kumari, V. Verma, S. Nimesh, Recent development in therapeutic strategies targeting *Pseudomonas aeruginosa* biofilms – A review. *Mater. Today Proc.* **46**, 2359–2373 (2021).
56. J. Y. Co, T. Crouzier, K. Ribbeck, Probing the role of mucin-bound glycans in bacterial repulsion by mucin coatings. *Adv. Mater. Interfaces* **2**, 1500179 (2015).
57. A. N. Kwant *et al.*, Sticky science: Using complex coacervate adhesives for biomedical applications. *Adv. Healthc. Mater.* **2402340**, 1–13 (2024).
58. B. X. Wang *et al.*, Mucin glycans signal through the sensor kinase RetS to inhibit virulence-associated traits in *Pseudomonas aeruginosa*. *Curr. Biol.* **31**, 90–102 (2021).
59. J. Y. Co *et al.*, Mucins trigger dispersal of *Pseudomonas aeruginosa* biofilms. *npj Biofilms Microbiomes* **4**, 23 (2018).
60. R. Hartmann *et al.*, Quantitative image analysis of microbial communities with BiofilmQ. *Nat. Microbiol.* **6**, 151–156 (2021).